Chinese Journal of Chemical Engineering 84 (2025) 96–106

Contents lists available at ScienceDirect

Chinese Journal of Chemical Engineering

journal homepage: www.elsevier.com/locate/CJChE

Full Length Article

Process fault root cause diagnosis through state evolution mapping based on temporal unit shapelets

Zhenhua Yu [1], Guan Wang [2], Qingchao Jiang [1,*], Xuefeng Yan [1]

[1] Key Laboratory of Smart Manufacturing in Energy Chemical Process, Ministry of Education, East China University of Science and Technology, Shanghai 200237, China

[2] State Key Laboratory of Bioreactor Engineering, East China University of Science and Technology, Shanghai 200237, China

ARTICLE INFO

Article history:
Received 3 September 2024
Received in revised form
18 April 2025
Accepted 20 April 2025
Available online 14 May 2025

Keywords:
Root cause diagnosis
Neural networks
Shapelet
Fermentation
Bioprocess

ABSTRACT

Accurate fault root cause diagnosis is essential for ensuring stable industrial production. Traditional methods, which typically rely on the entire time series and overlook critical local features, can lead to biased inferences about causal relationships, thus hindering the accurate identification of root cause variables. This study proposed a shapelet-based state evolution graph for fault root cause diagnosis (SEG-RCD), which enables causal inference through the analysis of the important local features. First, the regularized autoencoder and fault contribution plot are used to identify the fault onset time and candidate root cause variables, respectively. Then, the most representative shapelets were extracted to construct a state evolution graph. Finally, the propagation path was extracted based on fault unit shapelets to pinpoint the fault root cause variable. The SEG-RCD can reduce the interference of noncausal information, enhancing the accuracy and interpretability of fault root cause diagnosis. The superiority of the proposed SEG-RCD was verified through experiments on a simulated penicillin fermentation process and an actual one.

© 2025 The Chemical Industry and Engineering Society of China, and Chemical Industry Press Co., Ltd. All rights are reserved, including those for text and data mining, AI training, and similar technologies.

1. Introduction

The failure to promptly identify and rectify production faults could lead to substantial economic losses and even pose threats to human safety [1–5]. Fault root cause diagnosis (RCD) focuses on determining the fundamental sources of faults in industrial processes and tracing the trajectories of fault propagation. As such, it has attracted significant attention from researchers and industry practitioners [6]. Conventional RCD methods, which include signed directed graphs [7,8], adjacency matrices [9], fault trees [10], and process causality diagrams [11–13], are all grounded in the mechanics of industrial processes and expert knowledge. Consequently, data-driven approaches have increasingly come to the forefront.

In recent years, unsupervised methods that use causal diagrams of process variables have become the preferred approach for RCD. Among these methods, Granger causality (GC) has received significant attention [14–16]. For instance, Yuan *et al.* [17] identified data with prominent resonance characteristics through latent variable techniques, subsequently leveraging both time-domain and spectral GC for precise detection of oscillation origins. Another method, which employed statistical tests to assess the nonstationary or nonlinear nature of time series, integrates Gaussian process regression with multivariate causal analysis to overcome the limitations of traditional GC, which primarily applies to stable and linear time series [18]. To address the challenges of processing nonlinear signals and their inclination toward generating extraneous causal links, a method combining recursive neural networks with GC has been proposed [19]. Another study introduced a method that integrates 1D convolution with graph attention networks and uses causal graphs derived from conditional GC analysis to facilitate prompt RCD following fault identification [20]. Song *et al.* [21] proposed a causal source consistency analysis (CSCA) framework to achieve time-frequency collaboration. Zhao *et al.* [22] characterized the direct and indirect GC through multi-level predictive relationships, thus fully describing the root cause variables.

Apart from GC, the transfer entropy has also been widely used in RCD. Shu *et al.* [23] modified the primitive transfer entropy to enhance its ability to detect time-delayed causality. Direct transfer entropy has been proposed to detect direct causal relationships [24]. Meanwhile, Li *et al.* [25] proposed a framework for steady-

This article is part of a special issue entitled: AI for Chemical Engineering published in Chinese Journal of Chemical Engineering.

* Corresponding author.
E-mail address: qchjiang@ecust.edu.cn (Q. Jiang).

https://doi.org/10.1016/j.cjche.2025.04.011
1004-9541/© 2025 The Chemical Industry and Engineering Society of China, and Chemical Industry Press Co., Ltd. All rights are reserved, including those for text and data mining, AI training, and similar technologies.

state and nonsteady-state fault RCD based on transfer entropy and GC. A data-driven RCD method measures the strength of causality by using normalized transfer entropy [26]. In addition, the effectiveness of GC and transfer entropy in industrial datasets has been validated [27]. However, GC assumes linear stationary causal relationships, while transfer entropy demands data that adherence to a defined probability model. These limitations constrain their applicability in complex industrial scenarios.

To address redundant causality in data, one method computes maximum spanning trees to convert causal analysis findings into directed acyclic graphs, thus reducing the effect of feedback controllers and recirculation on RCD [28]. Jiang *et al.* [29,30] proposed a technique based on partial cross mapping (PCM) to eliminate indirect causal relationships, thus eradicating all cycles within the mapping and facilitating accurate RCD. By using the Kolmogorov-Smirnov test to assess causal strength variations due to disturbances, a different method eliminates nonessential causal links by analyzing normal and fault data [31]. Although direct causality analysis methods can effectively remove the impact of redundant causality, the identification of root causes still entails significant complexity.

Song *et al.* [32] proposed a sparse time-varying relationship extraction method for the RCD of nonstationary processes. Wang *et al.* [33] introduced a data-driven RCD method, which enabled more accurate localization of fault origins and the identification of their propagation pathways in complex industrial environments. Zhou *et al.* [34] enhanced temporal convolutional networks for causal analysis through feature reconstruction and skip connections. Furthermore, they introduced a scoring rule for root nodes via contrastive causal graphs to RCD.

However, because these methods rely on complete time series and often overlook critical local features, they may compromise causal inference and thus fail to accurately identify the fault root cause variable [35,36]. Therefore, this study introduces a shapelet-based state evolution graph for fault root cause diagnosis (SEG-RCD), enhancing causal inference by focusing on significant local features. First, a regularized autoencoder (AE) and fault contribution plot were employed to determine the fault onset time and identify candidate root cause variables. Then, a state evolution graph was constructed using shapelets, from which the most representative shapelets were extracted. Finally, a propagation path graph was derived from the fault unit shapelets, enabling the precise identification of the root cause variable. The contributions of this work include the following:

1) A fault root cause diagnosis method based on significant local features is proposed, addressing biased causal inference caused by redundant temporal information.
2) The visualized shapelets improve the interpretability of root cause analysis results.
3) Two experiments were conducted and the superiority of the proposed method was verified.

The structure of this paper is organized as follows: Section 2 shows the preliminaries; Section 3 details the proposed method; Section 4 demonstrates the superiority of the proposed method through two experiments; Section 5 provides a summary.

2. Preliminaries

2.1. AE based fault detection

AE is an unsupervised learning approach that can be used for fault detection [37]. For a sample $\boldsymbol{x}$, the H^2 statistic can be obtained by

$$H^2 = \boldsymbol{z}^{\mathrm{T}}\boldsymbol{z} = \left(\sigma\left(\boldsymbol{W}^{(1)}\boldsymbol{x}+\boldsymbol{b}^{(1)}\right)\right)^{\mathrm{T}}\left(\sigma\left(\boldsymbol{W}^{(1)}\boldsymbol{x}+\boldsymbol{b}^{(1)}\right)\right) \tag{1}$$

and the Q statistic can be calculated as follows:

$$Q = (\boldsymbol{x}-\boldsymbol{x}')^{\mathrm{T}}(\boldsymbol{x}-\boldsymbol{x}') \tag{2}$$

where $\boldsymbol{x}' = \sigma(\boldsymbol{W}^{(2)}\boldsymbol{z}+\boldsymbol{b}^{(2)})$ is the reconstruction of $\boldsymbol{x}$, $\boldsymbol{z}$ is the hidden variable, $\boldsymbol{W}^{(1)}$, $\boldsymbol{W}^{(2)}$, $\boldsymbol{b}^{(1)}$ and $\boldsymbol{b}^{(2)}$ are parameters, $\sigma(\cdot)$ is the activation function. The loss function can be calculated as follows:

$$\mathcal{L}\left(\boldsymbol{W}^{(1)},\boldsymbol{W}^{(2)},\boldsymbol{b}^{(1)},\boldsymbol{b}^{(2)}\right) = \sum_{n=1}^{N}\left\|\boldsymbol{x}^{(n)}-\boldsymbol{x}'^{(n)}\right\|^2 \tag{3}$$

where N represents the number of sample. The thresholds H^2_{th} and Q_{th} are determined using kernel density estimation (KDE) [38]. Fault detection is achieved using the following logical discriminant:

$$\begin{cases} Q > Q_{\mathrm{th}} \text{ or } H^2 > H^2_{\mathrm{th}} \Rightarrow \text{fault} \\ Q \le Q_{\mathrm{th}} \text{ and } H^2 \le H^2_{\mathrm{th}} \Rightarrow \text{fault} - \text{free} \end{cases} \tag{4}$$

2.2. Dynamic time warping

Assuming there are time series segments $\boldsymbol{s}_i$ with length l_i and $\boldsymbol{s}_j$ with length l_j respectively, an alignment $\boldsymbol{a} = (\boldsymbol{a}_1, \boldsymbol{a}_2)$ is a combination of two index sequences of length p, that satisfies the following conditions:

$$\begin{aligned} &1 \le \boldsymbol{a}_k(1) \le \cdots \le \boldsymbol{a}_k(p) = l_k, \\ &\boldsymbol{a}_k(n+1) - \boldsymbol{a}_k(n) \le 1, \\ &\text{for } k = i, j, \text{and } 1 \le n \le p-1. \end{aligned} \tag{5}$$

The representation of all alignment schemes is denoted as $\boldsymbol{A}(\boldsymbol{s}_i, \boldsymbol{s}_j)$. Dynamic time warping (DTW) links a specific point in one sequence to consecutive points in another, as illustrated in Fig. 1.

$$d_{\mathrm{DTW}}(\boldsymbol{s}_i, \boldsymbol{s}_j) = \min_{\boldsymbol{a}\in\boldsymbol{A}(\boldsymbol{s}_i,\boldsymbol{s}_j)} \tau(\boldsymbol{s}_i, \boldsymbol{s}_j|\boldsymbol{a}). \tag{6}$$

In the above equation, $\tau(\boldsymbol{s}_i, \boldsymbol{s}_j|\boldsymbol{a})$ represents the distance between two sequences under the alignment $\boldsymbol{a}$, in which the alignment that yields the minimum distance being denoted as $\boldsymbol{a}^*$.

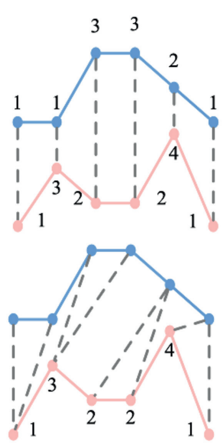

B \ A	1	1	3	3	2	1
1	0	0	2	4	5	5
3	2	2	0	0	1	3
2	3	3	1	1	0	1
2	4	4	2	2	0	1
4	7	7	3	3	2	3
1	7	7	5	5	3	2

Fig. 1. The diagram of dynamic time warping.

3. Method

3.1. Overview

The SEG-RCD mainly consists of three components: offline modeling, online monitoring and root cause diagnosis, as illustrated in Fig. 2.

When conducting fault root cause diagnosis, the first step is to apply Eqs. (1) and (2) to construct the H^2 and Q statistics. Considering the similarity of data between batches, a parameter regularization term is incorporated into Eq. (3) when constructing the AE-based fault monitoring model to enhance generalization.

$$\mathcal{L}(\boldsymbol{\theta}) = \sum_{n=1}^{N} \left\| \boldsymbol{x}^{(n)} - \boldsymbol{x}'^{(n)}(\boldsymbol{\theta}) \right\|^2 + \lambda \|\boldsymbol{\theta}\| \tag{7}$$

where $\boldsymbol{\theta} = \{\boldsymbol{W}^{(1)}, \boldsymbol{W}^{(2)}, \boldsymbol{b}^{(1)}, \boldsymbol{b}^{(2)}\}$, λ is the penalty coefficient, $\boldsymbol{x}^{(n)}$ represents the truth of the n-th sample, $\boldsymbol{x}'^{(n)}(\boldsymbol{\theta})$ represents the reconstructed value of n-th sample with parameter $\boldsymbol{\theta}$, N represents the number of sample, n represent the index of the sample. Next, the fault onset time is determined using Eq. (4). Upon fault detection, the fault contribution plot is used to identify candidate root cause variables. The distance between shapelets and segments can be redefined as shown in Eq. (8).

$$\widehat{d}(\boldsymbol{v}, \boldsymbol{s}|\xi) = \tau(\boldsymbol{v}, \boldsymbol{s}|\boldsymbol{a}^*, \xi) = \sqrt{\sum_{k=1}^{p} \xi_{\boldsymbol{a}_1^*}(k) \cdot \left(\boldsymbol{v}_{\boldsymbol{a}_1^*(k)} - \boldsymbol{s}_{\boldsymbol{a}_2^*(k)} \right)^2} \tag{8}$$

where ξ represents a local factor indicating the internal importance of a specific shapelet, $\boldsymbol{a}^*$ represents the best alignment. Furthermore, a global factor ψ to capture the influence across segments,

$$\widehat{d}(\boldsymbol{v}, \boldsymbol{t}|\xi, \psi) = \min_{1 \le k \le m} \psi_k \cdot \widehat{d}(\boldsymbol{v}, \boldsymbol{s}_k|\xi) \tag{9}$$

where $\boldsymbol{t}$ is partitioned into m segments, denoted as $\boldsymbol{t} = \{s_1, \cdots, s_m\}$.

The parameters ξ and ψ in Eq. (9) can be learned through classifying tasks, and the temporal unit shapelets are extracted to construct the state evolution graph. Specifically, assuming there are C categories, the loss function is defined in a one *vs* all format, as shown in Eq. (10).

$$L_{\text{category}} = -\sum_{c=1}^{C} D_{\text{KL}}(d_{\text{DTW}}(\boldsymbol{v}, T_c) \| d_{\text{DTW}}(\boldsymbol{v}, T \backslash T_c)) \tag{10}$$

where T_c represents the sample set of the category c, $T \backslash T_c$ represents the sample set of all other categories except for c, D_{KL} represents the KL divergence. It should be noted that DTW is not a differentiable operation and cannot be optimized by gradient descent methods, so we used soft-DTW instead of DTW [39]. Then the top K representative shapelets can be extracted through minimizing Eq. (11).

$$L_{\text{total}} = L_{\text{category}} + \alpha\|\xi\| + (1-\alpha)\|\psi\| \tag{11}$$

where α is a trade-off hyperparameter.

Each time series segment $\boldsymbol{s}_i$ is assigned to the nearest shapelet, with the assignment probabilities normalized as follows:

$$p_{i,j} = \frac{\max\left(\widehat{d}_{i,*}(\boldsymbol{v}_{i,*}, \boldsymbol{s}_i)\right) - \widehat{d}_{i,j}(\boldsymbol{v}_{i,j}, \boldsymbol{s}_i)}{\max\left(\widehat{d}_{i,*}(\boldsymbol{v}_{i,*}, \boldsymbol{s}_i)\right) - \min\left(\widehat{d}_{i,*}(\boldsymbol{v}_{i,*}, \boldsymbol{s}_i)\right)} \tag{12}$$

where $\boldsymbol{v}_{i,*}$ represents the shapelets assigned to segment $\boldsymbol{s}_i$, $\boldsymbol{v}_{i,j}$ is the j-th assignment of $\boldsymbol{s}_i$, $\boldsymbol{p}_{i,*}$ represents the probability of $\boldsymbol{v}_i$ is assigned to $\boldsymbol{s}_i$, and

$$\widehat{d}_{i,*}(\boldsymbol{v}_{i,*}, \boldsymbol{s}_i) = \psi_*(i) \cdot \widehat{d}\left(\boldsymbol{v}_{i,*}, \boldsymbol{s}_i | \xi^*\right) \tag{13}$$

Eq. (12) connects shapelets of adjacent segments, allowing the calculation of the transition probability from one shapelet to the next.

For each pair (j,k), the weighted edge from $\boldsymbol{v}_{i,j}$ to $\boldsymbol{v}_{i+1,k}$ is created by

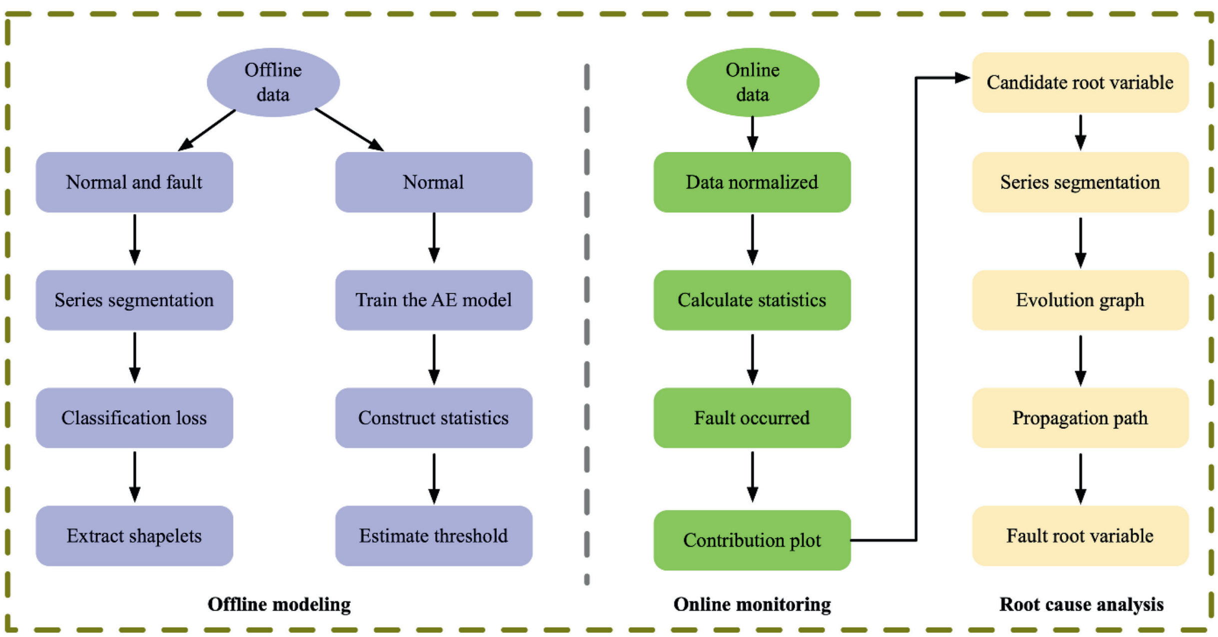

Fig. 2. The flowchart of the SEG-RCD method.

$$\boldsymbol{w}_{i,j\rightarrow i+1,k} = \boldsymbol{p}_{i,j} \cdot \boldsymbol{p}_{i+1,k} \tag{14}$$

then, a directed graph $G = (V, E)$ is established, where $V = \{v_{i,j} : i \in [1, N], j \in [1, K]\}$ and $E = \{\boldsymbol{e}_{i,j\rightarrow i+1,k}, \forall (i, j, k)\}$, with K most representative shapelets as its vertices and directed edge weights of $\boldsymbol{p}_{i,j} \cdot \boldsymbol{p}_{i+1,k}$, i.e,

$$\boldsymbol{e}_{i,j\rightarrow i+1,k} = \left(\boldsymbol{v}_{i,j}, \boldsymbol{v}_{i+1,k}, \boldsymbol{w}_{i,j\rightarrow i+1,k}\right) \tag{15}$$

The candidate root cause variables are obtained from the fault contribution plot, taking l points before and after their fault time points t_{f} to form the fault unit $\mathcal{F}_i$,

$$\mathcal{F}_i = \left\{x_i(t) : t \in \left[t_{\mathrm{f}} - l, t_{\mathrm{f}} + l\right]\right\} \tag{16}$$

where $x_i(t)$ represents the observation data at time point t of the i-th candidate root cause variables. The shapelet closest to the unit on G is selected as the vertex to construct a fault propagation path graph,

$$v_{i,j}^{\mathrm{f}} = \underset{v_{i,j} \in V}{\operatorname{argmin}} \widehat{d}\left(v_{i,j}, \mathcal{F}_i | \xi, \psi\right) \tag{17}$$

Then, the fault propagation path graph $G_{\mathrm{f}} = (V_{\mathrm{f}}, E_{\mathrm{f}})$ is extracted from G, where $V_{\mathrm{f}} = \{v_{i,j}^{\mathrm{f}}\}$ is the vertice on G_{f}, and E_{f} is the edge between these vertices. Identify the fault variables with information flowing in but not out as the root cause variable,

$$\mathcal{R} = \left\{v \in V_{\mathrm{f}} | \mathrm{In-degree}(v) = 0 \;\text{ and }\; \mathrm{Out-degree}(v) > 0\right\} \tag{18}$$

where $\mathcal{R}$ represents the identified root cause variables. The proposed method is illustrated in detail in Algorithm 1 and Fig. 3.

Algorithm 1: SEG-RCD

Offline modeling
1) Determine H_{th}^2 and Q_{th} based on Eqs. (1)–(3) and KDE method.
2) Calculate the distance between shapelets and segments based on Eqs. (8) and (9) using both normal and fault data simultaneously.
3) Select the K shapelets with the smallest loss based on Eqs. (10) and (11).

Online monitoring
1) Plot the fault monitoring diagram and determine the fault time based on Eqs. (1)–(4).
2) Identifying candidate fault root cause variables based on the fault contribution plot.

Root cause diagnosis
1) Build a system state evolution diagram based on Eqs. (12)–(15).
2) Calculate the faulty units for each variable according to Eq. (16)
3) Obtain the fault variable state evolution graph according to Eq. (17).
4) Identify the fault root cause variable according to Eq. (18).

3.2. Characteristic analysis

The advantages of the SEG-RCD can be summarized as follows: First, the SEG-RCD utilizes shapelets to capture local patterns in

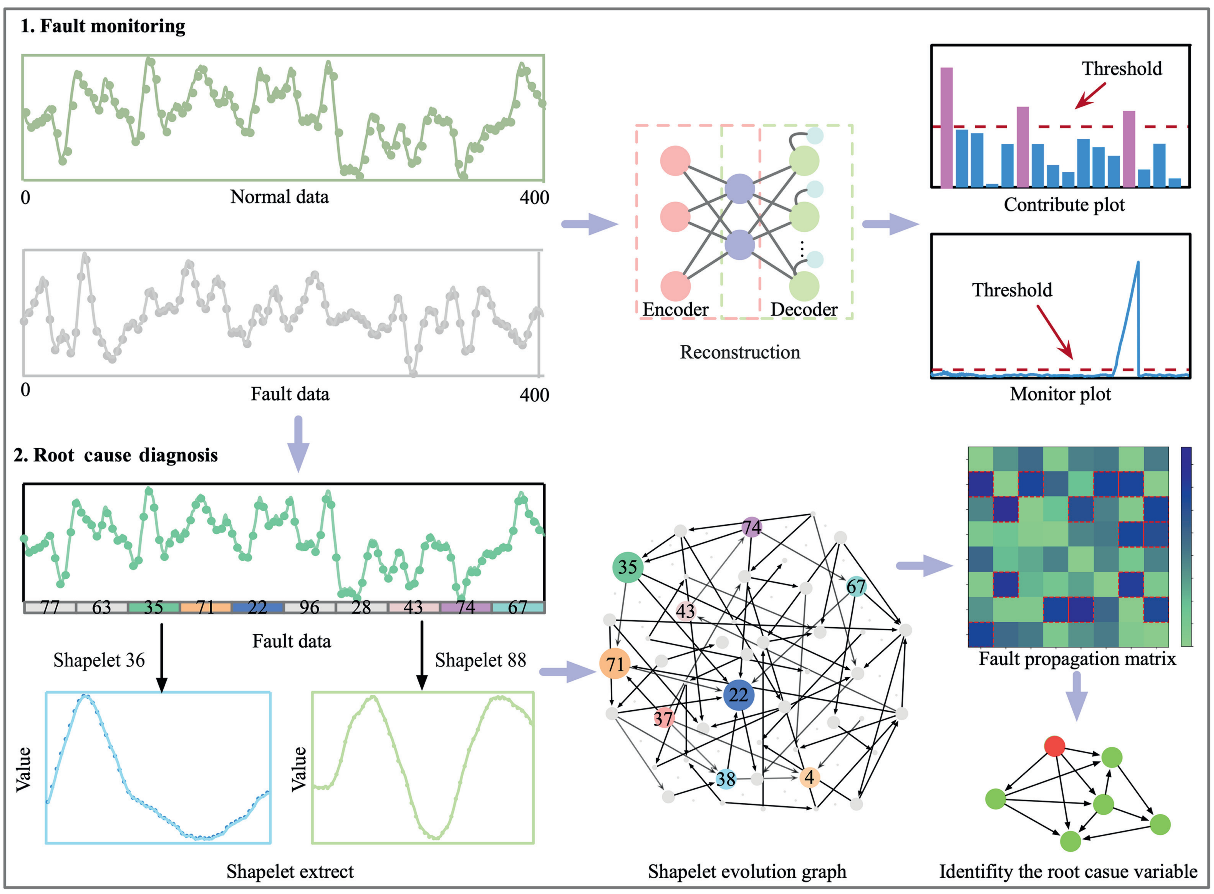

Fig. 3. The detailed procedure of the proposed SEG-RCD.

time-series data, effectively addressing nonlinear relationships, particularly in scenarios where the data distribution may evolve over time. By incorporating regularization terms (such as penalties), the model's generalization capability is enhanced, thereby improving its robustness to uncertainty and noise. Moreover, the shapelet extraction process facilitates the identification of more discriminative features from the data, further increasing the stability and accuracy of the method. The visualization and interpretability of the shapelets contribute to the clarity and transparency of fault diagnosis results, thus significantly improving the interpretability of the method.

4. Case Study

4.1. Penicillin fermentation simulation

The simulation data were derived from the Pensim 2.0 simulation platform developed by Cinar [40]. The simulation flowchart is shown in Fig. 4.

The penicillin simulation spanned 400 h, and the data was collected at uniform 1-h intervals. This process generated 16 variables, with 10 variables are commonly used for concise analysis as shown in Table 1.

Three types of faults were introduced into the system, as shown in Table 2.

As shown in Fig. 5, the proposed fault monitoring method accurately detects the onset time of fault 2 and fault 3. For fault 1, there is a slight delay between the detected fault onset time and the truth due to its nature as a slope fault, which has small fluctuations at the onset, making it difficult to distinguish. However, this delay does not significantly impact root cause tracing results, as the total length of data before and after the fault is considered. In addition, it should be noted that the regularized AE can be replaced with other advanced monitoring algorithms capable of calculating fault contribution to adapt root cause diagnosis across different datasets.

Table 1
The 10 variables used in the penicillin fermentation simulation.

No.	Variable	No.	Variable
1	Aeration rate	6	DO
2	Agitator power	7	Culture volume
3	Substrate feed flow rate	8	CO_2 concentration
4	Substrate feed temperature	9	pH
5	Substrate concentration	10	Temperature

Table 2
Details of three faults introduced into the simulation.

Fault no.	Fault variable	Fault description	Fault time
1	Aeration rate	+5% Ramp change	300
2	Agitator power	−10% Step change	200
3	Substrate feed flow rate	+5% Step change	50

The results of the normalized variable fault contribution by AE under the three faults are shown in Fig. 6. Although there are some more advanced methods in the field of fault isolation [41], the fault contribution plot performs well in terms of computational efficiency and adaptability to AE based fault detection methods. Therefore, this study adopted the fault contribution plot to determine the candidate root cause variables. To verify the superiority of the SEG-RCD, eight variables with the highest fault contribution were selected for the next analysis. According to Fig. 6, the candidate root cause variables of fault 1 are [x_1, x_2, x_3, x_4, x_5, x_7, x_8, x_{10}], while those for faults 2 and 3 are [x_1, x_2, x_3, x_4, x_5, x_6, x_7, x_8].

The results of using GC, PCM and SEG-RCD for fault root cause diagnosis are presented in Fig. 7. After the causal graph is drawn, the root cause variable was identified using Eq. (18); specifically, a variable with no incoming fault information and only outputs is considered as the root cause variable. For GC and PCM, we determine the optimal embedding dimension using the false nearest neighbor algorithm and select the time lag corresponding to the first

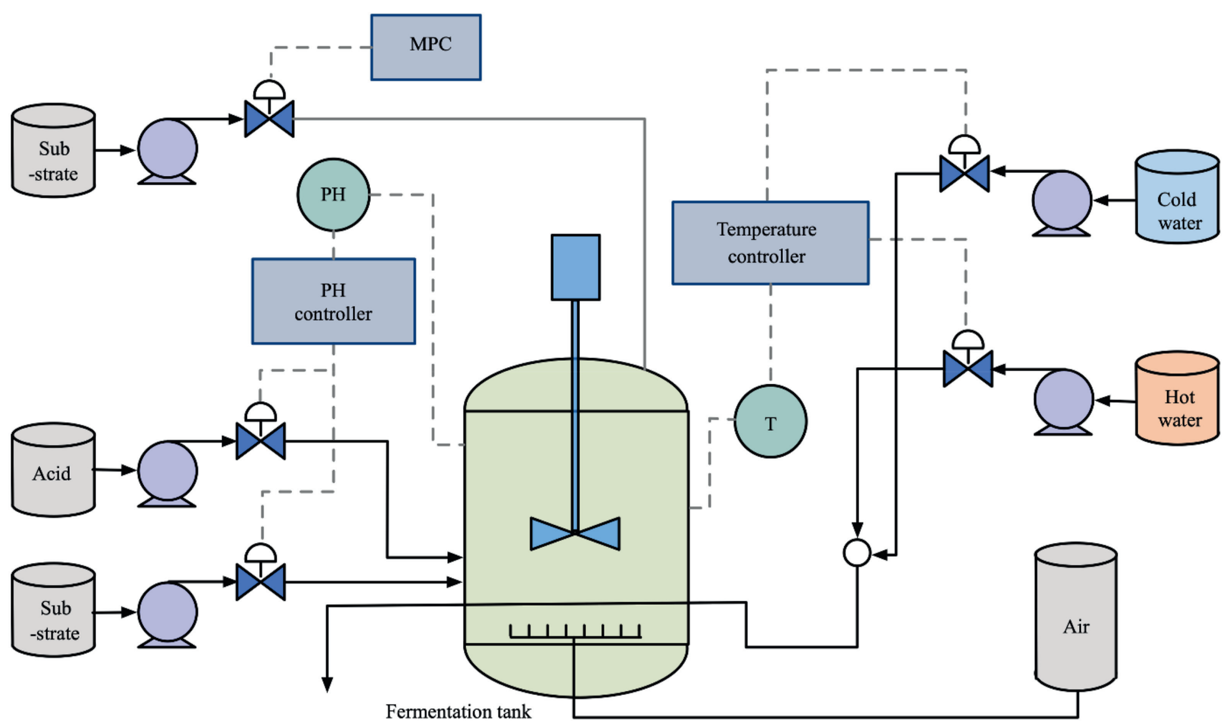

Fig. 4. Flowchart of the penicillin fermentation simulation.

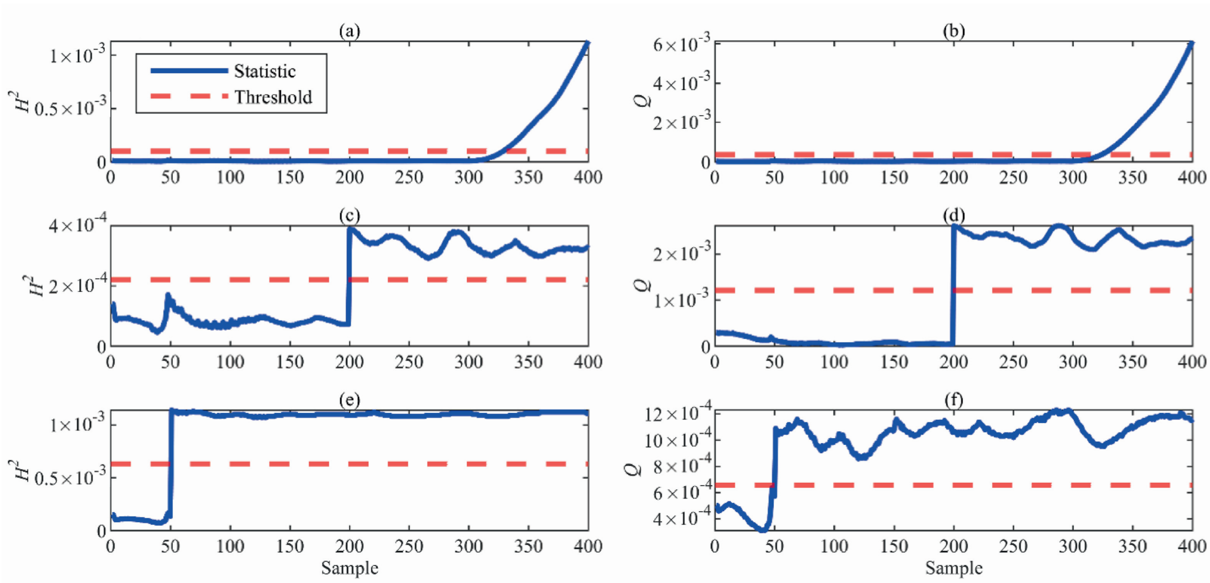

Fig. 5. Monitoring results on penicillin simulation process: (a) fault 1 H^2, (b) fault 1 Q, (c) fault 2 H^2, (d) fault 2 Q, (e) fault 3 H^2, (f) fault 3 Q.

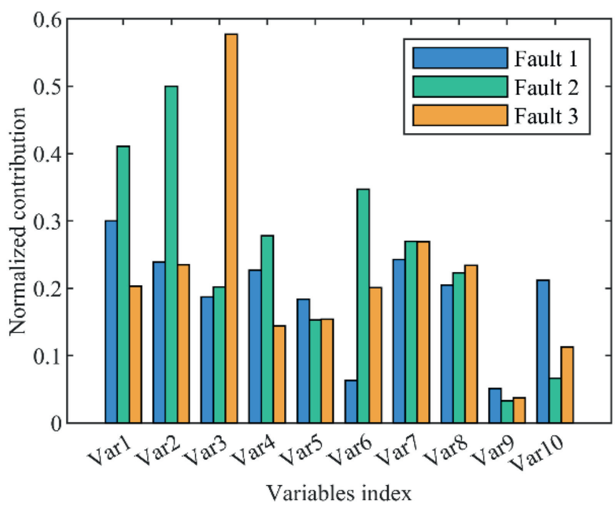

Fig. 6. The fault contribution plot of the three faults.

minimum of delayed mutual information. Additionally, we test the hypothesis that Y does not Granger cause X and infer direct causal relationships by applying the F-statistic with a 95% significance level. Specifically, for the simulation, we use an embedding dimension of 2 and a time lag of 2. The parameters of SEG-RCD were selected through grid search, with a learning rate set to 0.01. As shown in Fig. 7(a), despite the differences in the fault propagation paths identified by the three methods, x_1 only has output and no information inflow among all causal graphs. This indicates that the fault variable identified by all three methods are x_1. Indeed, a ramp fault was introduced into aeration rate during the simulation. Thus, all methods successfully identify the root cause variable for fault 1. As seen in Fig. 7(b), the fault root cause variable identified by GC is x_4, while PCM and SEG-RCD both identify x_2 as the fault root cause variable. Indeed, a step change fault was introduced into agitator power. Thus, only PCM and SEG-RCD correctly identify the root dependent variable for fault 2. From Fig. 7(c), it is easy to see that only SEG-RCD can correctly identify the root cause variable of fault 3.

In summary, when three different types of faults are introduced in the penicillin simulation, the GC perform poorly and can only identify the root cause variables when fault 1 occurs. Meanwhile, the performance of PCM is barely satisfactory, as it can only identify the root cause variables of fault 1 and fault 2. In comparison, the method with the best performance is our proposed SEG-RCD, which can identify the root cause variables of all three types of faults. To explain the superiority of the SEG-RCD, several shapelets selected by SEG-RCD are visualized in Fig. 8.

From Fig. 8(a), the shapes of x_1 and x_{10} are recognized as monotonically increasing, which conforms to the characteristics of fault 1. In Fig. 8(b), the step descent characteristic is captured by the shapelet of x_2. In Fig. 8(c), the feature of x_3 is recognized as a step rise by the shapelet feature, which in turn leads to an increase in x_8. This is also in line with common sense that the increase of substrate feed temperature increases the reaction rate, thereby producing more CO_2.

The proposed SEG-RCD method can structure fault propagation paths that align with common sense and correctly identify the root cause variable. Furthermore, the shapelets extracted by SEG-RCD effectively capture significant changes in the fault time series of the penicillin simulation. In the following analysis, SEG-RCD will be applied to an actual penicillin fermentation process to demonstrate its superiority in identifying changes under real operating conditions.

4.2. Real penicillin fermentation process

The actual penicillin fermentation data used in this study was obtained from the National Biotechnology Engineering Research Center in Shanghai, China. The production process is depicted in Fig. 9.

Experimental research was conducted using process data from two batches of an actual penicillin fermentation process. Table 3 presents the fault information, where changes in operating conditions between different batches are considered as production faults. Consequently, each fault is named according to its batch.

Faults 21a and 21b replicate the production process of the batch 16b with the difference that sugar and nutrients are added after

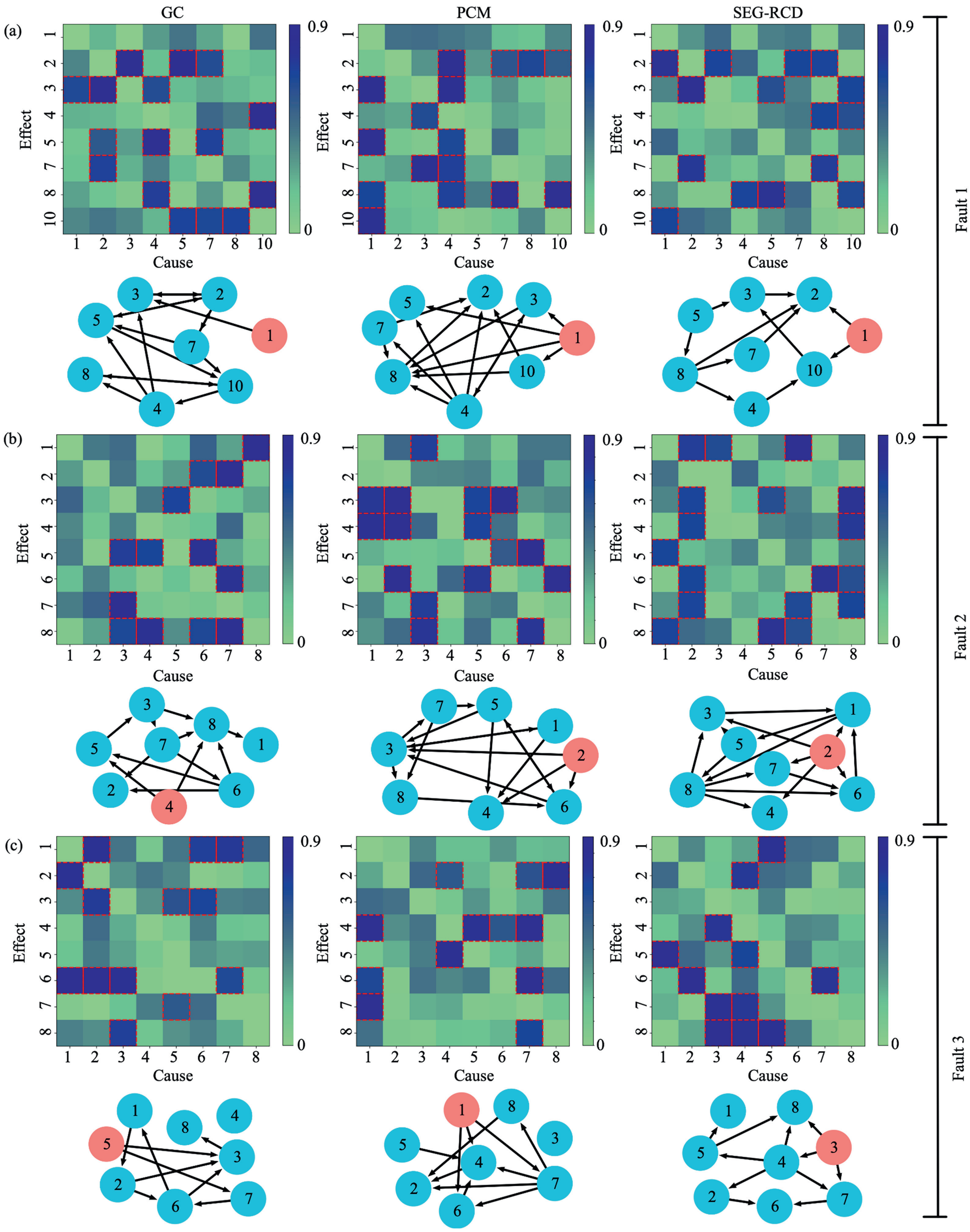

Fig. 7. The propagation and root cause variable in simulation case: (a) fault 1, (b) fault 2, (c) fault 3.

100 h. Based on experts' experience, 15 variables (shown in Table 4) were selected for the subsequent analysis. The batch data were augmented using generative models to obtain more samples for shapelets extraction.

As shown in Fig. 10, the proposed regularized AE can accurately detect the time when the operating conditions change during the actual production process. Similar to the experiment conducted in the penicillin simulation process, the AE model can be substituted

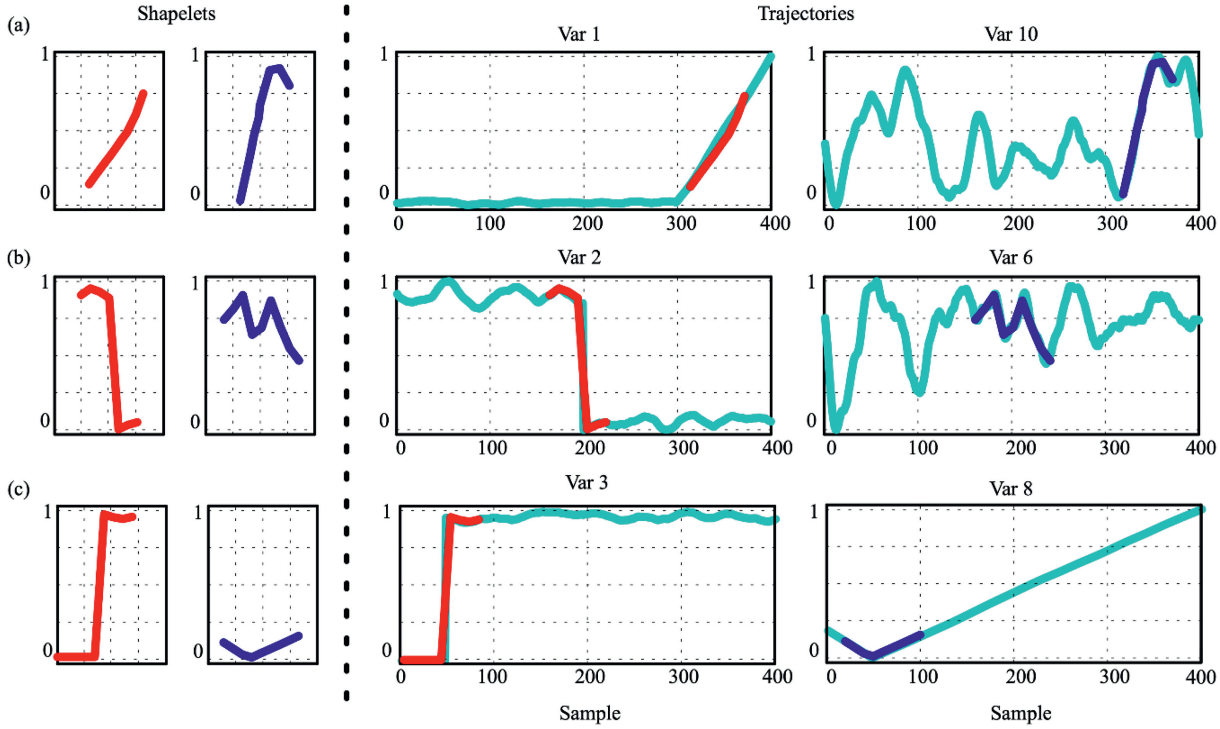

Fig. 8. Several key shapelets in the simulation: (a) fault 1, (b) fault 2, (c) fault 3.

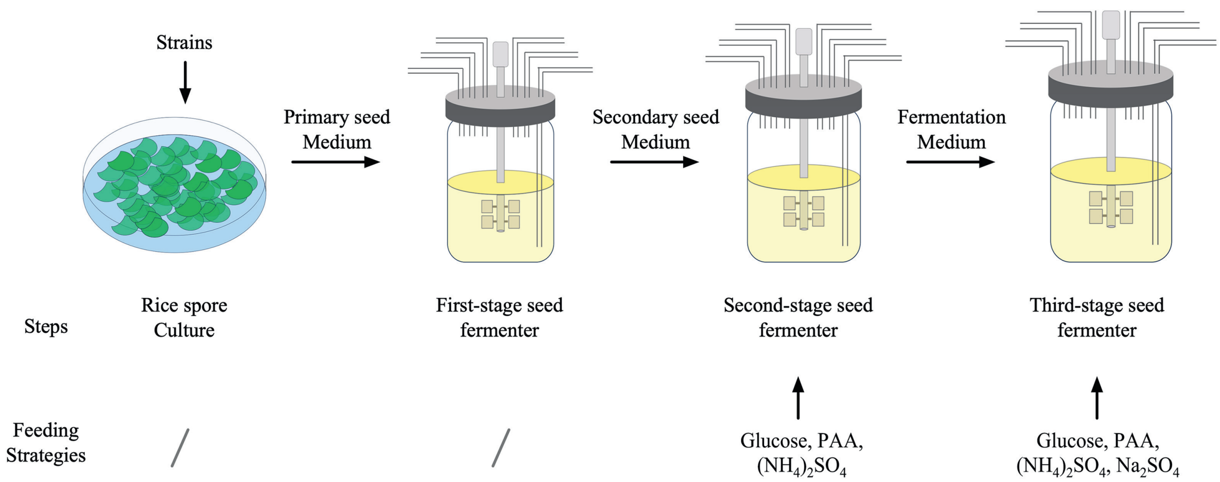

Fig. 9. Flowchart of real penicillin fermentation process.

with other advanced monitoring models based on specific practical requirements.

The normalized fault contribution plots for faults 21a and fault 21b are presented in Fig. 11. The [x_1, x_2, x_3, x_4, x_5, x_6, x_8, x_{11}] and [x_1, x_2, x_3, x_4, x_7, x_8, x_9, x_{12}] were selected as candidate root cause variables for 21a and 21b, respectively. The fault root diagnosis results are shown in Fig. 12.

In the experiment of real penicillin fermentation process data, the determination of parameters for different methods is the same as the simulation process. Specifically, we use embedding

Table 3
Fault information on the real penicillin fermentation process.

Fault	Interval	Size	Description
21a	1 min	11339	Add sugar
21b	1 min	12384	Add all materials

Table 4
The 15 selected variables in the real penicillin fermentation process.

No.	Variable	No.	Variable
1	Temperature	9	Tank pressure
2	Dissolved oxygen	10	Accumulated phenylacetic acid
3	PH	11	Accumulated sodium sulfate
4	Volume	12	Accumulated ammonium sulfate
5	Tail oxygen	13	OUR
6	Tail carbon	14	CER
7	Accumulated ammonia water	15	KLA
8	Accumulated sugar water		

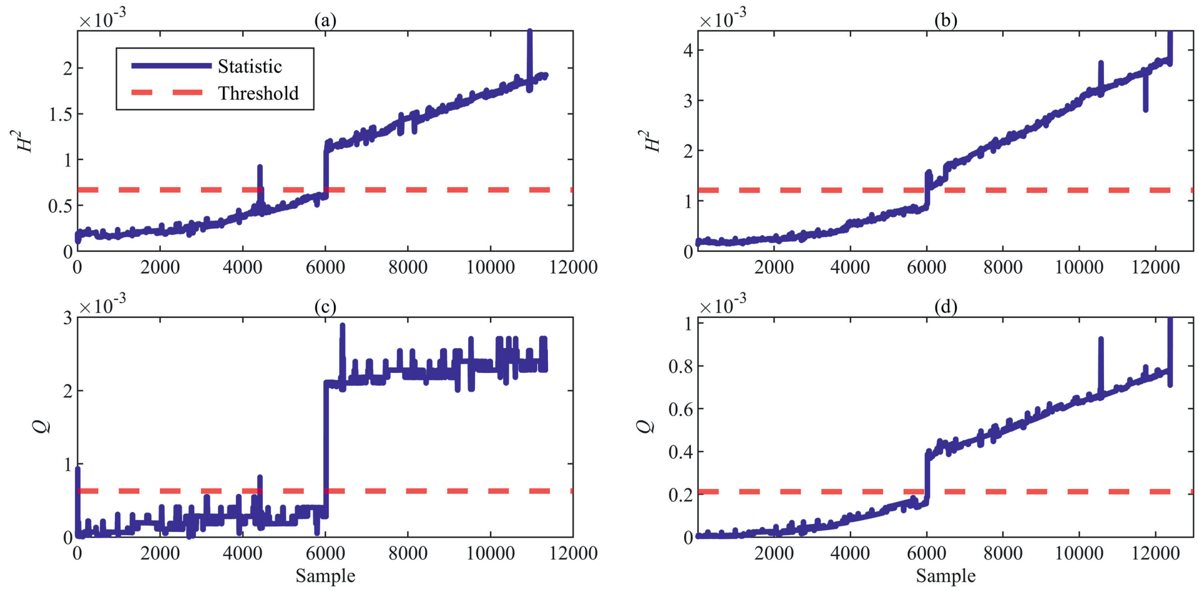

Fig. 10. Monitoring chart on real penicillin fermentation process: (a) fault 21a H^2, (b) fault 21b H^2, (c) fault 21a Q, (d) fault 21b Q.

dimension 3 and time lag 2 for the real process, the learning rate of the SEG-RCD is 0.01. In Fig. 12(a), the root cause variable identified by GC is x_6, by PCM is x_6 and x_4, and SEG-RCD is x_8. However, in the actual production process, the changed operating condition of 21a is the sugar supplementation rate, which means the actual root cause variable is x_8. Therefore, for fault 21a, only SEG-RCD correctly identified the root cause variable under real production conditions. For fault 21b, the actual operating conditions were changed to supplement nutrients. After a similar analysis of Fig. 12(b), it was found that only SEG-RCD identified x_9 as the root cause variable, which aligns with the actual data acquisition method. Based on the above analysis, it can be concluded that for the two faults of real penicillin fermentation process, the GC and PCM are unable to identify variables affected by changes in operating conditions. However, SEG-RCD can accurately identify the root cause variable.

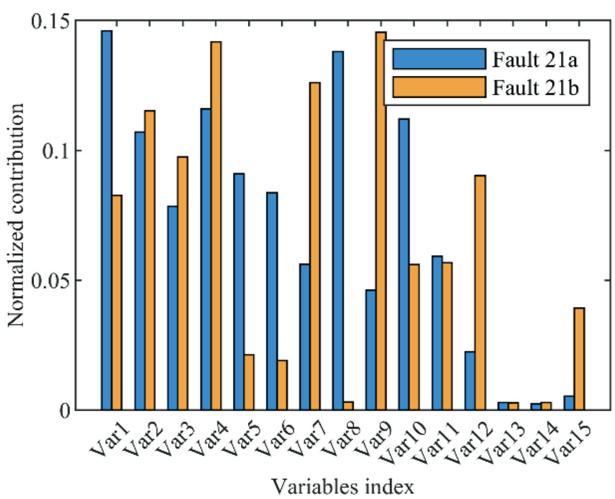

Fig. 11. The fault contribution plots of faults 21a and 21b.

The key shapelets are visualized and analyzed using a method similar to that applied in the simulation process, as shown in Fig. 13.

In Fig. 13(a), the shapelets of x_5, x_6, and x_8 show an upward trend in all three variables following increased sugar supplementation. This can be explained by the increase in sugar supplementation, which leads to an accumulation of sugar water, subsequently causing an increase in tail oxygen and tail carbon. In Fig. 13(b), the shapelet of x_9 captures the increase in tank pressure resulting from the addition of supplementary materials, which causes a pressure rise, promotes the reaction, and leads to an increase in volume. Thus, the proposed SEG-RCD algorithm successfully identifies the root cause, and the extracted shapelets precisely delineate the critical changes in variables.

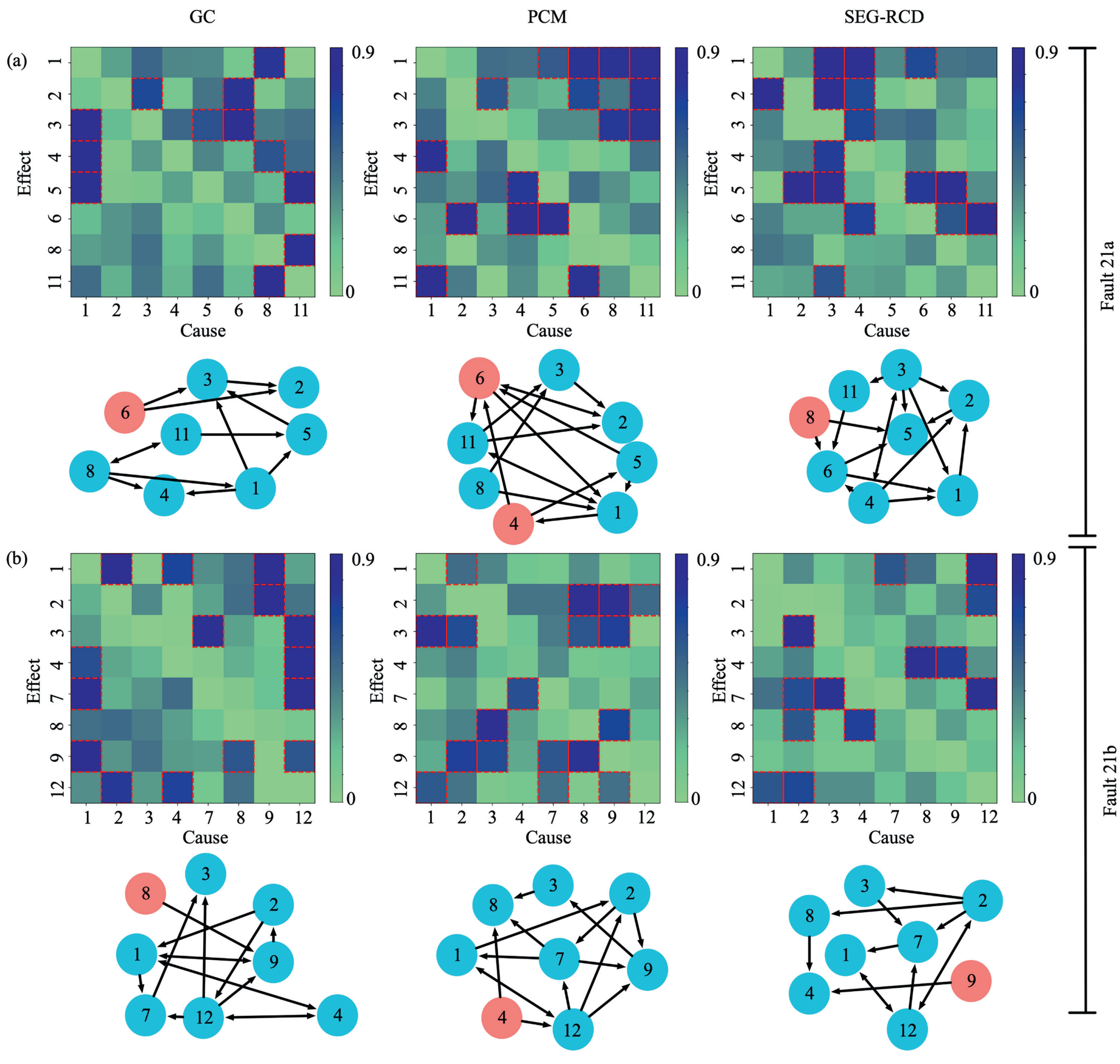

Fig. 12. The propagation and root cause variables in the actual penicillin fermentation process: (a) fault 21a, (b) fault 21b.

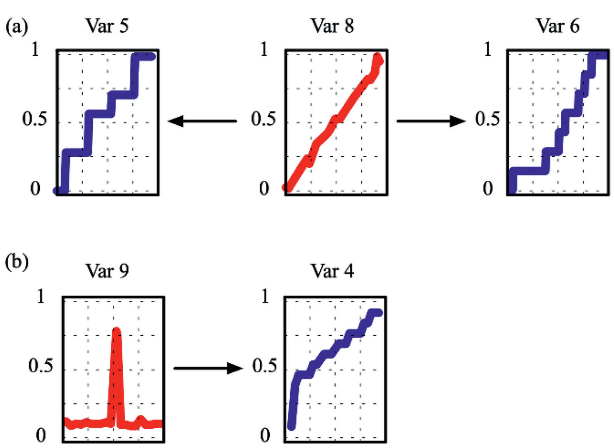

Fig. 13. The key shapelets in the real process: (a) fault 21a, (b) fault 21b.

5. Conclusions

This study presents a method named SEG-RCD, which can identify the fault root cause variable in industrial process and possess interpretable ability. By utilizing AE and state evolution graphs based on shapelets, the proposed method employs a fault contribution plot to identify the candidate fault variables. The most representative shapelets were selected from the time series segments to construct a state evolution graph, which can effectively trace the fault propagation pathway and ultimately identify the root cause variable. When implemented on both simulated and real penicillin fermentation datasets, the proposed method has been proven to be more superior to existing granger causality and partial cross mapping. In particular, by using shapelets that represent the state of variables, rather than using all the available data, the proposed method constructs a causal diagram, which successfully identifies both the root cause variables of faults in the simulation process and the variables that change operating conditions in the actual production process. In addition, the extracted shapelets can accurately characterize the key features of the time series after the fault occurs. Overall, the insights derived from the proposed SEG-RCD can uncover critical process information within the penicillin fermentation process, thereby supporting the refinement of current control strategies. Although the SEG-RCD has shown superiority in root cause fault diagnosis and interpretability, it still cannot infer polarity. Future research will focus on studying causal diagram construction methods that can determine causal polarity between variables, further enhancing interpretability.

CRediT Authorship Contribution Statement

Zhenhua Yu: Writing – original draft, Methodology, Investigation, Conceptualization. Guan Wang: Validation, Resources, Data curation. Qingchao Jiang: Writing – review & editing, Supervision, Project administration, Methodology, Conceptualization. Xuefeng Yan: Writing – review & editing, Supervision, Methodology.

Declaration of Competing Interest

The authors declare that they have no known competing financial interests or personal relationships that could have appeared to influence the work reported in this paper.

Acknowledgements

The authors gratefully acknowledge the support from the following foundations: the National Natural Science Foundation of China (62322309, 62433004), Shanghai Science and Technology Innovation Action Plan (23S41900500), and Shanghai Pilot Program for Basic Research (22TQ1400100-16).

References

[1] H. Safaeipour, M. Forouzanfar, A. Casavola, A survey and classification of incipient fault diagnosis approaches, *J. Process Control* 97 (2021) 1–16.
[2] L.M. Elshenawy, T.A. Mahmoud, Fault diagnosis of time-varying processes using modified reconstruction-based contributions, *J. Process Control* 70 (2018) 12–23.
[3] J.J. Luo, Z.H. Jin, H.P. Jin, Q. Li, X. Ji, Y.Y. Dai, Causal temporal graph attention network for fault diagnosis of chemical processes, *Chin. J. Chem. Eng.* 70 (2024) 20–32.
[4] J.X. Zhang, W.J. Luo, Y.Y. Dai, Y.M. Yao, Cycle temporal algorithm-based multivariate statistical methods for fault diagnosis in chemical processes, *Chin. J. Chem. Eng.* 47 (2022) 54–70.
[5] L.Y. Jiang, L. Xie, S.Q. Wang, Fault diagnosis for batch processes by improved multi-model fisher discriminant analysis, *Chin. J. Chem. Eng.* 14 (3) (2006) 343–348.
[6] X. Zhao, W.W. Yan, H.H. Shao, Monitoring and fault diagnosis for batch process based on feature extract in fisher subspace, *Chin. J. Chem. Eng.* 14 (6) (2006) 759–764.
[7] M. Ram Maurya, R. Rengaswamy, V. Venkatasubramanian, Application of signed digraphs-based analysis for fault diagnosis of chemical process flowsheets, *Eng. Appl. Artif. Intell.* 17 (5) (2004) 501–518.
[8] D. Gao, C.G. Wu, B.K. Zhang, X. Ma, Signed directed graph and qualitative trend analysis based fault diagnosis in chemical industry, *Chin. J. Chem. Eng.* 18 (2) (2010) 265–276.
[9] H.L. Jiang, R. Patwardhan, S.L. Shah, Root cause diagnosis of plant-wide oscillations using the concept of adjacency matrix, *J. Process Control* 19 (8) (2009) 1347–1354.
[10] S. Kabir, An overview of fault tree analysis and its application in model based dependability analysis, *Expert Syst. Appl.* 77 (2017) 114–135.
[11] Y.M. Wan, F. Yang, N. Lv, H.P. Xu, H. Ye, W.C. Li, P. Xu, L.M. Song, A.K. Usadi, Statistical root cause analysis of novel faults based on digraph models, *Chem. Eng. Res. Des.* 91 (1) (2013) 87–99.
[12] L.H. Chiang, B.B. Jiang, X.X. Zhu, D.X. Huang, R.D. Braatz, Diagnosis of multiple and unknown faults using the causal map and multivariate statistics, *J. Process Control* 28 (2015) 27–39.
[13] J. Dong, K.R. Cao, K.X. Peng, Hierarchical causal graph-based fault root cause diagnosis and propagation path identification for complex industrial process monitoring, *IEEE Trans. Instrum. Meas.* 72 (2023) 3513911.
[14] C.W.J. Granger, Investigating causal relations by econometric models and cross-spectral methods, *Econometrica* 37 (3) (1969) 424.
[15] J.F. Geweke, Measures of conditional linear dependence and feedback between time series, *J. Am. Stat. Assoc.* 79 (388) (1984) 907–915.
[16] L. Barnett, A.K. Seth, The MVGC multivariate Granger causality toolbox: a new approach to Granger-causal inference, *J. Neurosci. Methods* 223 (2014) 50–68.
[17] T. Yuan, S.J. Qin, Root cause diagnosis of plant-wide oscillations using Granger causality, *IFAC Proc.* 45 (15) (2012) 160–165.
[18] H.S. Chen, Z.B. Yan, Y. Yao, T.B. Huang, Y.S. Wong, Systematic procedure for granger-causality-based root cause diagnosis of chemical process faults, *Ind. Eng. Chem. Res.* 57 (29) (2018) 9500–9512.
[19] G. Shen, P.L. Wang, K.L. Hu, Q.Y. Ye, Fault root cause diagnosis method based on recurrent neural network and granger causality. 2021 CAA Symposium on Fault Detection, Supervision, and Safety for Technical Processes (SAFEPROCESS), IEEE, Chengdu, China, 2021.
[20] Y.X. Liu, B. Jafarpour, Graph attention network with Granger causality map for fault detection and root cause diagnosis, *Comput. Chem. Eng.* 180 (2024) 108453.
[21] P.Y. Song, C.H. Zhao, B. Huang, Addressing heterogeneous time-frequency causality: source consistency exploring for industrial root cause alignment and diagnosis, *IEEE Trans. Cybern.* 55 (3) (2025) 1107–1120.
[22] P.Y. Song, C.H. Zhao, B. Huang, MPGE and RootRank: a sufficient root cause characterization and quantification framework for industrial process faults, *Neural Netw.* 161 (2023) 397–417.
[23] Y.D. Shu, J.S. Zhao, Data-driven causal inference based on a modified transfer entropy, *Comput. Chem. Eng.* 57 (2013) 173–180.
[24] P. Duan, F. Yang, T.W. Chen, S.L. Shah, Direct causality detection *via* the transfer entropy approach, *IEEE Trans. Control Syst. Technol.* 21 (6) (2013) 2052–2066.
[25] G. Li, S.J. Qin, T. Yuan, Data-driven root cause diagnosis of faults in process industries, *Chemometr. Intell. Lab. Syst.* 159 (2016) 1–11.
[26] B. Rashidi, D.S. Singh, Q. Zhao, Data-driven root-cause fault diagnosis for multivariate non-linear processes, *Control Eng. Pract.* 70 (2018) 134–147.
[27] P. Duan, T.W. Chen, S.L. Shah, F. Yang, Methods for root cause diagnosis of plant-wide oscillations, *AIChE J.* 60 (6) (2014) 2019–2034.
[28] Y. Liu, H.S. Chen, H.B. Wu, Y. Dai, Y. Yao, Z.B. Yan, Simplified Granger causality map for data-driven root cause diagnosis of process disturbances, *J. Process Control* 95 (2020) 45–54.
[29] Q.C. Jiang, W.J. Wang, S.T. Chen, C.J. Pan, W.M. Zhong, Hierarchical fault root cause identification in plant-wide processes using distributed direct causality analysis, *IEEE Trans. Ind. Inf.* 20 (3) (2024) 3232–3241.
[30] Q.C. Jiang, J.S. Jiang, W.J. Wang, C.J. Pan, W.M. Zhong, Partial cross mapping based on sparse variable selection for direct fault root cause diagnosis for industrial processes, *IEEE Transact. Neural Networks Learn. Syst.* 35 (5) (2024) 6218–6230.
[31] J.G. Wang, R. Chen, X.Y. Ye, Y. Yao, Z.T. Xie, S.W. Ma, L.L. Liu, Data-driven root cause diagnosis of process disturbances by exploring causality change among variables, *J. Process Control* 129 (2023) 103062.
[32] P.Y. Song, C.H. Zhao, B. Huang, M. Wu, Sparse and time-varying predictive relation extraction for root cause quantification of nonstationary process faults, *IEEE Trans. Instrum. Meas.* 71 (2022) 3525013.
[33] S. Wang, Q. Zhao, Y.H. Han, J.K. Wang, Root cause diagnosis for process faults based on multisensor time-series causality discovery, *J. Process Control* 122 (2023) 27–40.
[34] Y.J. Zhou, K. Xu, F. He, Root cause diagnosis in multivariate time series based on modified temporal convolution and multi-head self-attention, *J. Process Control* 117 (2022) 14–25.
[35] Z.Q. Cheng, Y. Yang, W. Wang, W.J. Hu, Y.T. Zhuang, G.J. Song, Time2Graph: revisiting time series modeling with dynamic shapelets, *Proc. AAAI Conf. Artif. Intell.* 34 (4) (2020) 3617–3624.
[36] L.X. Ye, E. Keogh, Time series shapelets: a novel technique that allows accurate, interpretable and fast classification, *Data Min. Knowl. Discov.* 22 (1) (2011) 149–182.
[37] W.W. Yan, P.J. Guo, L. gong, Z.K. Li, Nonlinear and robust statistical process monitoring based on variant autoencoders, *Chemometr. Intell. Lab. Syst.* 158 (2016) 31–40.
[38] E. Parzen, On estimation of a probability density function and mode, *Ann. Math. Stat.* 33 (3) (1962) 1065–1076.
[39] M. Cuturi, M. Blondel, Soft-DTW: a Differentiable Loss Function for time-series 1703, 2017 01541.
[40] G. Birol, Ü. Cenk, Ç. Ali, A modular simulation package for fed-batch fermentation: penicillin production, *Comput. Chem. Eng.* 26 (11) (2002) 1553–1565.
[41] P.Y. Song, C.H. Zhao, B. Huang, J.L. Ding, Explicit representation and customized fault isolation framework for learning temporal and spatial dependencies in industrial processes, *IEEE Transact. Neural Networks Learn. Syst.* 35 (3) (2024) 2997–3011.